

## Contribution to the study of the coexistence of phases tetragonal-rhombohedral in ceramic type PZT and general form: $\text{Pb} [\text{Zr}_x\text{Ti}_{0.95-x}(\text{Mo}_{1/3}\text{In}_{2/3})_{0.05}]\text{O}_3$

M. Abba<sup>a</sup>, Z. Necira, N. Abdessalem and A Boutarfaia

Laboratory of Applied Chemistry, Department of Science Matter, University of Biskra, BP.145, RP-Biskra (07000), Algeria

**Abstract.**  $\text{Pb}[\text{Zr}_x\text{Ti}_{0.95-x}(\text{Mo}_{1/3}\text{In}_{2/3})_{0.05}]\text{O}_3$  piezoelectric ceramics with varying Zr/Ti ratio were prepared by the conventional method of thermal synthesis of mixed-oxides. The samples structures was determined by X-ray diffractometry to demonstrate the co-existence of the tetragonal and rhombohedral phases. In the present system the MPB, in which the tetragonal and rhombohedral phases coexist, is in a composition range of  $0.47 \leq x \leq 0.50$ . The lattice constants of the a and c axes for the samples caculeted from the XRD patterns. Microstructure of the sintered ceramics was observed by scanning electron microscopy (SEM) using free surfaces of the specimens.

**Keywords:** Morphotropic phase boundary; sintering temperature; Zr/Ti ratio.

### 1 Introduction

Lead zirconate titanate  $\text{Pb}(\text{Zr},\text{Ti})\text{O}_3$ , a solid solution of perovskite ferroelectric  $\text{PbTiO}_3$  and anti-ferroelectric  $\text{PbZrO}_3$  with different Zr/Ti ratio, is an important material that is widely used in electronic sensors, actuators, resonators and filters[1-3]. The materials with a perovskite structure of general formula  $\text{ABO}_3$  (where A = mono or divalent ions, B = tri, tetra or pentavalent ions) have been found to be very useful and interesting for different solid-state devices [4–8]. By making suitable substitution at A and/or B-site of  $\text{ABO}_3$  structure, a large number of charge neutral or deficient compounds have been prepared [9–11], which have been found to be very suitable and useful for many industrial applications.

In order to satisfy the requirements of practical applications of ultrasonic motors, many ternary and quaternary solid-solution, such as  $\text{Pb}(\text{Mn}_{1/3}\text{Nb}_{2/3})\text{O}_3$ -PZT,  $\text{Pb}(\text{Mn}_{1/3}\text{Sb}_{2/3})\text{O}_3$ -PZT,  $\text{Pb}(\text{Cd}_{1/3}\text{Nb}_{2/3})\text{O}_3$ -PZT,  $\text{Pb}(\text{Mn}_{1/3}\text{Nb}_{2/3})(\text{Ni}_{1/3}\text{Nb}_{2/3})\text{O}_3$ -PZT have been synthesized by modification or substitution[12-18].

The influence of technological factors on the width of the co-existence region was investigated on the ternary system  $\text{Pb}[\text{Zr}_x\text{Ti}_{(0.95-x)}(\text{Mo}_{1/3}, \text{In}_{2/3})_{0.05}]\text{O}_3$  by X-ray diffraction by varing the ratio Zr/Ti. The purpose of this work is to study the influence of sintering temperature on density, porosity and grain size on the ceramic, in order to determine the width of co-existence of tetragonal and rhombohedral phases and the exact composition of the MPB.

---

<sup>a</sup> e-mail : [abbamalika@gmail.com](mailto:abbamalika@gmail.com)

## 2 Experimental

All of the specimens were prepared by conventional ceramics technologie. The compositions of the Pb  $[\text{Zr}_x\text{Ti}_{(0.95-x)}(\text{Mo}_{1/3}\text{In}_{2/3})_{0.05}]\text{O}_3$  system were with  $46 \leq x \leq 55$ . The commercially available PbO,  $\text{ZrO}_2$ ,  $\text{TiO}_2$ ,  $\text{MoO}_3$  and  $\text{In}_2\text{O}_3$ , were used as the raw materials. Mixed oxides, after milling, were calcined at  $800^\circ\text{C}$  for 2h at heating and cooling rates of  $2^\circ\text{C}/\text{min}$ . After calcinations, the ground and milled powders were pressed into disks 13 mm in diameter and about 1 mm in thickness. Pressed disks of  $3\text{PbO} + 2\text{ZrO}_2$  placed in a capped crucible to prevent PbO evaporation during sintering. Four sintering conditions were selected to be used with both methods ranging 1000, 1100, 1150, and  $1180^\circ\text{C}$  for 2 h.

The crystal structure of the samples was analyzed using an X-ray diffractometry (XRD; Siemens D500). The voltage and currents ratings used were 40 kV, 30 mA respectively, and  $\text{CuK}\alpha$  radiation was used. The diffraction data were collected with an X-ray scan speed of  $0.1^\circ.\text{min}^{-1}$ . The bulk density was measured using the Archi-medes method.

## 3 Results and discussion

Sintered powders were examined by X-ray diffractometry to ensure phase purity and to identify the phases. The phases of the samples were detected using XRD (at room temperature) for several compositions given in Table 1.

**Table 1:** Series of compositions and crystal structure.

Sample	Crystal structure			
	1000 °C	1100 °C	1150 °C	1180 °C
$\text{Pb}[\text{Zr}_{0.46}\text{Ti}_{0.49}(\text{Mo}_{1/3}\text{In}_{2/3})_{0.05}]\text{O}_3$	T	T	T	T
$\text{Pb}[\text{Zr}_{0.47}\text{Ti}_{0.48}(\text{Mo}_{1/3}\text{In}_{2/3})_{0.05}]\text{O}_3$	T+R	T	T	T+R
$\text{Pb}[\text{Zr}_{0.49}\text{Ti}_{0.46}(\text{Mo}_{1/3}\text{In}_{2/3})_{0.05}]\text{O}_3$	T+R	T+R	T+R	T+R
$\text{Pb}[\text{Zr}_{0.50}\text{Ti}_{0.45}(\text{Mo}_{1/3}\text{In}_{2/3})_{0.05}]\text{O}_3$	T+R	T+R	T+R	T+R
$\text{Pb}[\text{Zr}_{0.51}\text{Ti}_{0.44}(\text{Mo}_{1/3}\text{In}_{2/3})_{0.05}]\text{O}_3$	T+R	T+R	T+R	R
$\text{Pb}[\text{Zr}_{0.52}\text{Ti}_{0.43}(\text{Mo}_{1/3}\text{In}_{2/3})_{0.05}]\text{O}_3$	T+R	T+R	T+R	R
$\text{Pb}[\text{Zr}_{0.54}\text{Ti}_{0.41}(\text{Mo}_{1/3}\text{In}_{2/3})_{0.05}]\text{O}_3$	T+R	T+R	R	R
$\text{Pb}[\text{Zr}_{0.55}\text{Ti}_{0.40}(\text{Mo}_{1/3}\text{In}_{2/3})_{0.05}]\text{O}_3$	R	R	R	R

T = Tetragonal; R = Rhombohedral; T-R = Tetragonal-Rhombohedral

It is reported that tetragonal, rhombohedral and T-R phases were identified by an analysis of the peaks 0 0 2 (tetragonal), 2 0 0 (tetragonal), 2 0 0 (rhombohedral)) in the  $2\theta$  range  $43-47^\circ$ .

The splitting of (0 0 2) and (2 0 0) peaks indicates that they are the ferroelectric tetragonal phase (T), while the single (2 0 0) peak shows the rhombohedral phase (R) (Figure1).

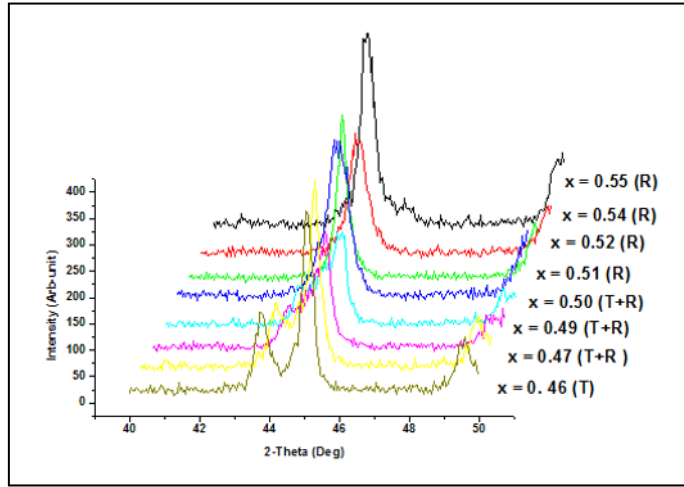


**Fig. 1:** The XRD patterns of Pb [Zr<sub>x</sub>Ti<sub>(0.95-x)</sub>(Mo<sub>1/3</sub>In<sub>2/3</sub>)<sub>0.05</sub>]O<sub>3</sub> system with 0.46 ≤ x ≤ 0.55.

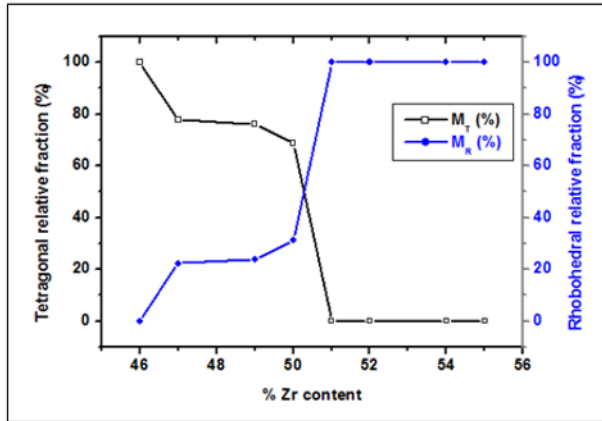
Triplet peaks indicate that the sample consists of a mixture of tetragonal and rhombohedral phases. The multiple peak separation method was used to estimate the relative fraction of coexisting phases. The relative phase fraction  $M_R$  and  $M_T$  were then calculated using the following equations [19]:

$$M_R = \frac{I_{R(200)}}{I_{R(200)} + I_{T(002)} + I_{T(200)}}$$

$$M_T = \frac{I_{T(200)} + I_{T(002)}}{I_{R(200)} + I_{T(002)} + I_{T(200)}}$$

Where  $I_{R(200)}$  is the integral intensity of the (200) reflection of the rhombohedral phase and  $I_{T(200)}$  and  $I_{T(002)}$  are the integral intensities of the (200) and (002) reflections of the tetragonal phase, respectively. A transition from tetragonal to rhombohedral phase is observed as Zr/Ti ratio increases. With increasing Zr/Ti ratio, tetragonal relative fraction decreases and rhombohedral relative fraction increases.

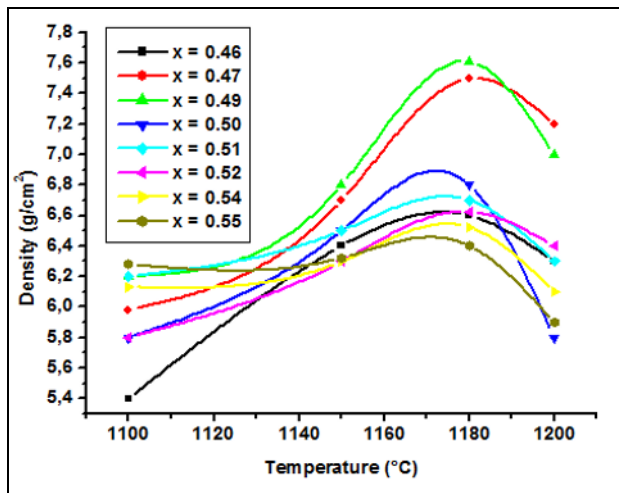
At 1180°C (Figure 2), It is shown that the tetragonal structure can be formed up to  $x_T > 0.46$  while the rhombohedral structure becomes stabilized for  $x_R < 0.51$ . However, at  $x = 0.46-0.51$ , tetragonal and rhombohedral phases coexist. The co-existence region is therefore quite narrow ( $\Delta x \approx 0.05$ ) and extends between  $x_T$  and  $x_R$ . The width  $\Delta x = x_T - x_R$  of the co-existence region from our work is close to that obtained by others [20,21]. The coexistence of tetragonal and rhombohedral phases has, therefore, to be attributed to the first order nature of the MPB, this is marked contrast to the proposition of Kakegawa et al.[22,23] that the coexistence is invariably due to compositional fluctuations.



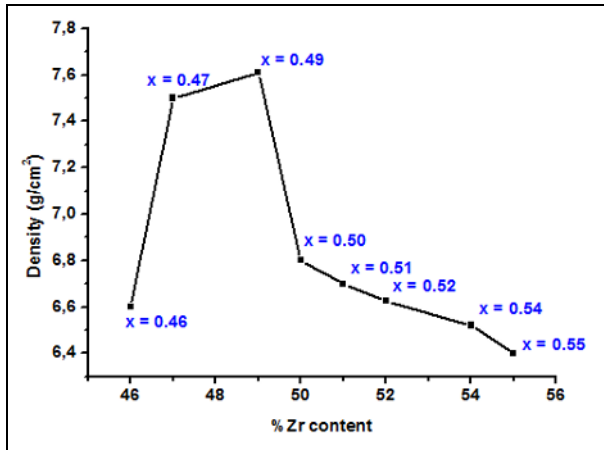
**Fig.2:** Variation of the relative content of the tetragonal and rhombohedral phases with different Zr% in the  $\text{Pb}[\text{Zr}_x\text{Ti}_{0.95-x}(\text{Mo}_{1/3}\text{In}_{2/3})_{0.05}]\text{O}_3$  (for a sintering temperature about  $1180^\circ\text{C}$ )

The study of density is necessary to optimize the optimum sintering temperature. Quality of the material increases with increasing density and it increases with increasing the sintering temperature [24]. The optimum temperature for sintering is determined from the pattern density as a function of sintering temperature  $d=f(T)$ . The maximum density is the product of better quality electrical (low dielectric loss). Figure 3. gathers the curves of the density of all samples depending on the sintering temperature. A similar shape for all curves: the density is minimal for a sintering temperature  $T = 1000^\circ\text{C}$ , it begins to grow until it reaches a maximum value at a sintering temperature  $T = 1180^\circ\text{C}$ , then it decreases the sintering temperature  $T = 1200^\circ\text{C}$  which means that the optimum temperature for sintering is  $1180^\circ\text{C}$ . Increased density means fewer and pore size, so the volume of the cell decreases and consequently the structure becomes more compact.

The optimum sintering temperature depends on several factors such as the addition of impurities, the rate of heating, time of thermal treatment and protecting atmosphere.

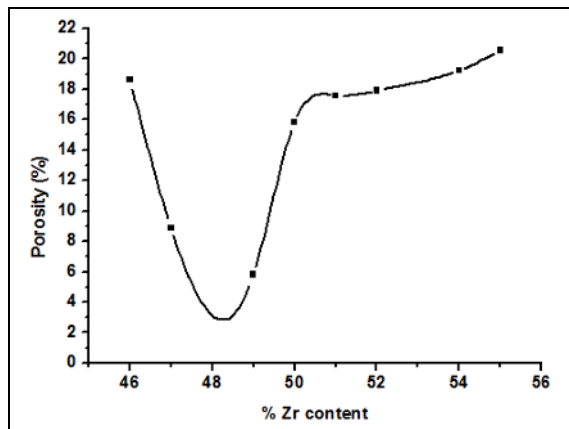


**Fig.3:** Effect of sintering temperature on density for  $\text{Pb}[\text{Zr}_x\text{Ti}_{0.95-x}(\text{Mo}_{1/3}\text{In}_{2/3})_{0.05}]\text{O}_3$



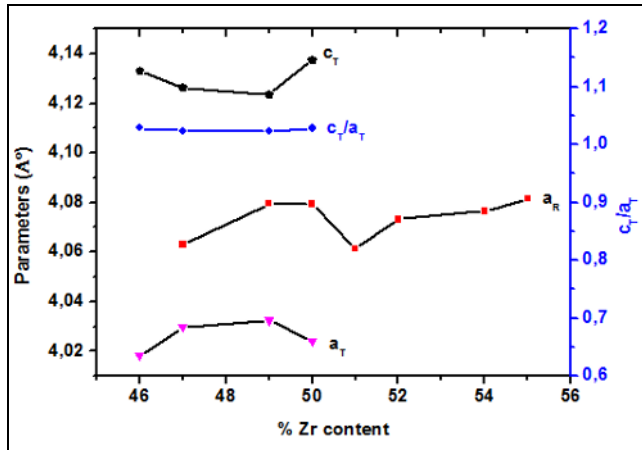
**Fig.4:** Evolution of density as a function of the concentration of Zr (%)

Changes in the density of different samples of  $Pb[Zr_xTi_{0.95-x}(Mo_{1/3}In_{2/3})_{0.05}]O_3$  Sintered at 1180 °C depending on the rate of Zr is shown in Figure 4. The shape of the curve shows that the density increases with increasing Zr concentration until a maximum value of 7.61g/cm<sup>3</sup> (94.18% of theoretical density) at Zr = 49% (sample No. 3) and then decreases.



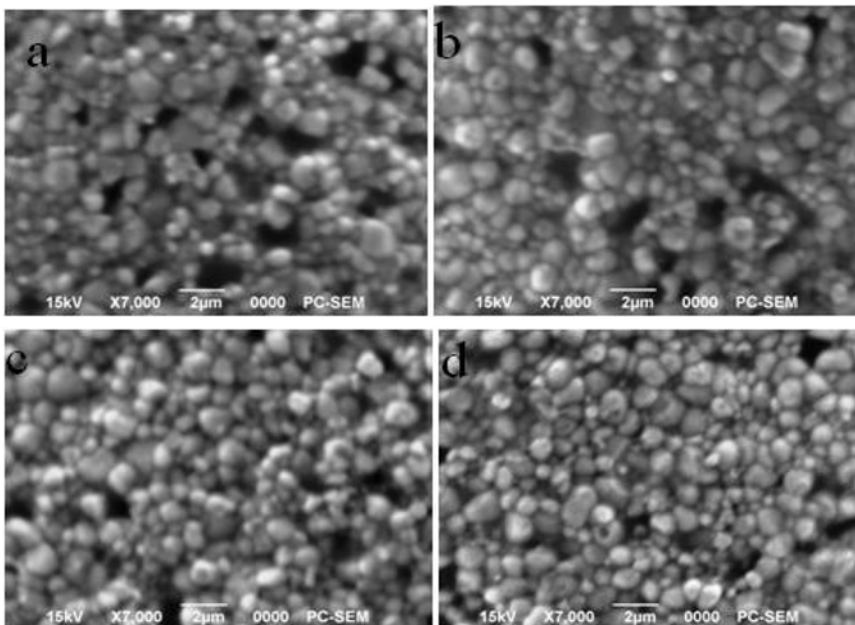
**Fig.5 :** the variation of porosity as a function of the concentration of Zr% for  $Pb[Zr_xTi_{0.95-x}(Mo_{1/3}In_{2/3})_{0.05}]O_3$  (for a sintering temperature about 1180°C).

Figure 5 shows the variation of the porosity for different samples depending on the concentration of Zr% and the sintering temperature of 1180 °C. Note that the porosity decreases until it reaches the minimum value  $p = 5.81\%$  for Zr = 0.49 (sample No. 3) and then increases.



**Fig.6:** The parameters of the lattice of  $\text{Pb}[\text{Zr}_x\text{Ti}_{0.95-x}(\text{Mo}_{1/3}\text{In}_{2/3})_{0.05}]\text{O}_3$  ceramics as a function of composition (for a sintering temperature about  $1180^\circ\text{C}$ ).

The parameters of the lattice were, then, determined from the triplets (200) by using a non-linear least squares method [25]. The  $a_R$ -parameter of the rhombohedral phase and the  $a_T$ -parameter,  $c_T$ -parameter, and the tetragonality ( $c_T/a_T$ ) of the tetragonal phase of  $\text{Pb}[\text{Zr}_x\text{Ti}_{0.95-x}(\text{Mo}_{1/3}\text{In}_{2/3})_{0.05}]\text{O}_3$  ceramics are plotted as a function of the ratio of Zr/Ti in Figure 6. The results showed that the parameters of the lattice of the tetragonal phase changed when the ratio of Zr/Ti was modified. While the value of the  $a_T$  parameter increased, the one of  $c_T$  parameter decreased, and the  $a_R$  parameter of the rhombohedral phase increased. The resulting values of the parameters of the lattice of the tetragonal phase showed that the  $c_T/a_T$  axial ratio decreased as  $a_T$  increased and  $c_T$  decreased. The values of the parameters of the lattice were revealed to be practically the same as those previously studied [26, 27].



**Fig.7:** SEM micrographs for  $\text{Pb}[\text{Zr}_{0.50}\text{Ti}_{0.45}(\text{Mo}_{1/3}\text{In}_{2/3})_{0.05}]\text{O}_3$  ceramics sintered at a)  $1000^\circ\text{C}$ , b)  $1100^\circ\text{C}$  c)  $1150^\circ\text{C}$  and d)  $1180^\circ\text{C}$ .

Figure 7, gives the SEM micrographs of free surfaces of the specimens sintered at 1000-1180°C for 2h. From these images, small crystallites with large pores for specimen sintered at 1000°C (Fig.7(a)) were noticed. As sintering temperature increased the grain grew and the average grain size increased slightly, whereas the number and the size of the pores decreased. The grain size exponentially increased with increasing temperature and this can be well explained by the phenomenological kinetic grain grow equation [28]. The average grain size is 1.15µm at temperature 1000 ° C which increases to 1.56 µm at temperature 1180 ° C.

## 4 Conclusion

In this study, ceramics in the  $\text{Pb}[\text{Zr}_x\text{Ti}_{0.95-x}(\text{Mo}_{1/3}\text{In}_{2/3})_{0.05}]\text{O}_3$  system (with  $0.46 \leq x \leq 0.55$ ) successfully prepared by a solid-state mixed-oxide technique. The co-existence region was investigated by X-ray diffraction. The study of the morphotropic phase boundary has established that the phase transition from tetragonal to rhombohedral symmetry takes place at  $x = 0.49$  and the width of the phase boundary has been found to be in the range of  $0.47 \leq x \leq 0.50$  at 1180°C.

The lattice parameters  $a_T$  and  $c_T$  of the tetragonal structure and  $a_R$  of the rhombohedral structure were found to change with composition. The effect of sintering temperature on the density and grain size has been investigated. It was demonstrated that the grain size and the density increased with increasing sintering temperature. The optimum sintering temperature (1180°C) corresponds to the maximum density, so the minimum value of porosity and also corresponds to the better quality product. To prove more my study, other measurements (dielectric, piezoelectric and hysteresis) should be done in the future.

## References

1. B.Jaffe, W. R. Cook, H. Jaffe, *Piezoelectric Ceramics* (Academic Press, New York, (1971).
2. T.Ezaki, S. Manuspiya, P. Moses, K. Uchino, V. Caraz, *Mater. Technol.* **19**, 79(2004).
3. K. Uchino, *Adv.Mater. Res.* **55-57**,1(2008).
4. J. Valasek, *Phys. Rev.*, **17**, 475(1921).
5. B. Wul, L.M. Goldman, *C.R. Acad. Sci., URSS* **46**,123 (1945).
6. S. Pilgrim, M. Audrey, E. Sutherland, E.R. Winzer, *J. Am. Ceram. Soc.*, **73**, 3122 (1990).
7. S. Miga, K. Wojcik, *Ferroelectrics* ,**100**,767 (1989).
8. K. L. Yadav, R.N.P. Choudhary, T.K. Chaki, *J. Mater. Sci.* **27**,5244(1992).
9. G. H. Heartling, *Ferroelectrics*, **75**,25 (1987).
10. L. Ramji, S.C. Sharma, D. Rajiv, *Ferroelectrics*, **100** ,43 (1989).
11. G.H. Heartling, *Ceramics Materials for Electronics* (Buchanan, New York (1991).
12. H. I. Chae, Y. S. Shin, K. J. Lim, H. D. Bae, D. W. Shin, *Proceedings of the fourth International Conference on Properties of Applied Dielectrics and Materials* (Brisbane, Australia, July 3-8, 1994).
13. L. Wu, C. K. Liang, C. F. Shieu, *J. Mater.Sci.* **26**,4439(1991).
14. J.S. Kim, S. J. Kim, H. J. Kim, D. C. Lee, K. Uchino, *Jpn. J. Appl. Phys.* **38**,1433(1999).
15. D. J. Lee, S. S. Kwon, S.H.Jeong, K.J. Lim, S.G. Park, H.H. Kim, T.Y. Lim, *Proceedings of the IEEE International Conference on Conduction and Breakdown in Solid Dielectric* (Vlisterris, Sweden, June 22-25, 1998).
16. X. H. Zhu, Z.Y. Meng, *J. Mate. Sci.* **31**,2171(1996).
17. X. B. Guo, H.Y. Chen, Z.Y. Meng, *Presented at the American Ceramic Society 103rd Annual Meeting, Indianapolis* (2000).
18. S. Tashiro, M. Ikehiro, H. Igarashi, *Jpn. J. Appl. Phys.* **36**,3004(1997).
19. G. H. Haerding and C.E. Land, *Soc.* **45**, 1-11(1974).
20. Y. Kala, *Phys. Status Solidi A* **87**,277 (1983).
21. K. Kakegawa, J. Mohri, V. Takahashi, K. Yamamura, Shirasaki, *Solid State Commun.***24**, 769(1977).

22. K. Kakegawa, J. Mohri, X. Shrasaki, K. Takahaashi, J. Am. Ceram. Soc. **24**, 515(1982).
23. W. Hammer, M.J Hoffmann, J. Electroceramics, **2**, 75(1998).
24. B. Jaff, W. R. Cook, H. Jaff, *Piezoelectric Ceramics*. Acadimic Press (London,U,K and N, U,1971).
25. B. D. Cullity, "*Elements of X-ray Diffraction* (Addison-Wesley Publishing Company, Inc., 1978).
26. Boutarfaia, Ceramics International, **26**, 583-587 (2000).
27. Boutarfaia, Ceramics International, **27**, 91-97 (2001).
28. T. Senda, R. C. Bradt, J. Am. Ceram. Soc, 73, 106-114 (1990).